Numerical Proof For Chemostat Chaos of Shilnikov's Type

Bo Deng[1], Maoan Han [2], Sze-Bi Hsu [3]

Abstract: A classical chemostat model is considered that models the cycling of one essential abiotic element or nutrient through a food chain of three trophic levels. The long-time behavior of the model was known to exhibit complex dynamics more than 20 years ago. It is still an open problem to prove the existence of chaos analytically. In this paper we aim to solve the problem numerically. In our approach we introduce an artificial singular parameter to the model and construct singular homoclinic orbits of the saddle-focus type which is known for chaos generation. From the configuration of the nullclines of the equations that generates the singular homoclinic orbits a shooting algorithm is devised to find such Shilnikov saddle-focus homoclinic orbits numerically which in turn imply the existence of chaotic dynamics for the original chemostat model.

Key Words: Chemostat model, Holling type II predation, Shilnikov's saddle-focus homoclinic orbit, chaos, shift dynamics, singular perturbation, shooting method

Lead Paragraph: **Chemostats are relatively easy to set up in laboratory to study microbial population interactions. A chemostat model was known for complex dynamics more than twenty years ago. But researchers have not come up with a mathematical proof for the suspected chaotic behavior. Reported here in this paper is the next-best solution for the problem, namely a computer-assisted proof for the existence of chaos outside the margins of numerical error. The strategy and method can be used to obtain conclusive proof** *in silico* **of chaos because mathematical proof is almost always next to impossible to construct for all physical systems.**

1. Introduction. A chemostat is a laboratory device consisting of three connected vessels. The first is the feed bottle contains all of the nutrients needed for the growth of a microorganism. The nutrient is pumped from the feed vessel into the culture vessel where the microorganisms grow and are well-mixed with nutrients. The third vessel is the overflow or collection vessel where nutrients, organisms and product produced pumped from the culture vessel. The chemostat is perhaps the best laboratory idealization of nature for population studies ([1, 2]). It is a dynamical system with continuous material input and output. The input and removal of nutrients mimic the continuous turnover of nutrients in nature. The washout of organisms is equivalent to non-age specific death, predation or emigration which always occurs in nature. The close parallels in nature are planktonic

[1]Mathematics and Science College, Shanghai Normal University, Shanghai, China, 200234, and Department of Mathematics, University of Nebraska-Lincoln, Lincoln, NE 68588, USA Email: bdeng@math.unl.edu

[2]Mathematics and Science College, Shanghai Normal University, Shanghai, China, 200234, Email: mahan@shnu.edu.cn

[3]Department of Mathematics, National Tsing-Hua University, Hsinchu, Taiwan 300, Email: sbhsu@math.nthu.edu.tw

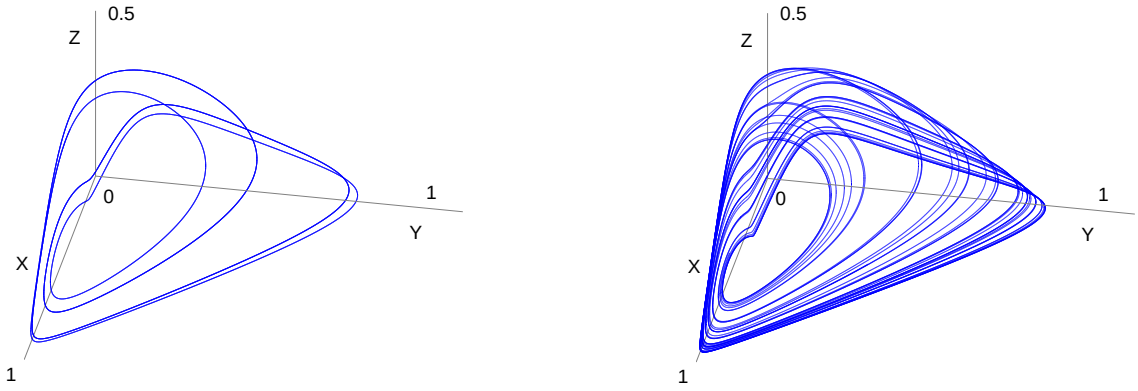

(a) (b)

Figure 1: The Smith-Waltman chemostat attractor of Eq.(5) for (a) $a_3 = 0.24$, (b) $a_3 = 0.2$, with all other parameter values: $a_1 = 0.08, a_2 = 0.23, m_1 = 10, m_2 = 4, m_3 = 3.5$.

communities of unicellular algae in lakes and oceans. The multiple species communities receive nutrient inputs from streams, draining watersheds or continental margins ([3]).

In this article we consider a three trophic levels food chain model in the chemostat with substrate (nutrient), producer (alga), consumer, predator. For the case of substrate-producer system one can show that either producer goes extinct (if the input concentration is too small to support the producer) or it converges to an equilibrium [4]. The survival of the organism satisfies an equation which is similar to a logistic equation. For the case of substrate-producer-consumer system, one can reduce it to a two-dimensional predator-prey system. It was analyzed in [5, 4] that either the solution converges to a positive equilibrium or there is a limit cycle. On the other hand, the predator-prey system with logistic growth for the prey and Holling type functional response for the predator satisfies that either the solution converges to a positive equilibrium or it converges to a unique limit cycle ([6, 7]). For one-prey-two-predator case, interested readers may consult the papers [8, 9, 10]. It is well-known ([11, 12, 13, 14, 15]) that for a prey-consumer-predator system with logistic growth for the prey, Holling type-II functional responses for the consumer and predator chaos may occur. In this article we study the substrate-producer-consumer-predator system in chemostat. By conservation of population densities, we reduce the system to producer-consumer-predator system. In their book [4](p.75) Smith and Waltman discovered a probable chaos in this closed system, see Fig.1. Since then researchers have wanted to answer the question whether their finds are merely periodic orbits or real chaotic attractors. But the problem remains open because proving chaos is always hard for differential equations.

The possibility that the model may only be capable of periodic orbits is not without his-

torical precedence in dynamical systems. After Smale proved that any arbitrary 3-dimensional smooth flow in a bounded region can be imbedded in a 4-dimensional competitive system ($x_i' = x_i N_i(x), \partial N_i(x)/\partial x_j \leq 0$ for $j \neq i$, $i = 1, 2, 3, 4$, [16]), the classical Lotka-Volterra system of competing species ([17, 18, 19]) gained considerable attention. With the discovery of Smale's horseshoe dynamics ([20]) that is embedded in the 3-dimensional Cartwright-Littlewood equations ([21, 22]), we know 4-dimensional competitive systems can be surely chaotic. That leads researchers to suspect that 3-dimensional competitive systems may be capable of dynamics more complex than periodicity. However, the 3-dimensional competitive LV system has now been classified into qualitative equivalence classes which can only have periodic cycles and equilibrium solutions, see [23] for more references. Nonetheless most researchers are agreed that the Smith-Waltman attractor is a chaotic kind because three-trophic food chain models are known to behave chaotically as early as 1978 ([12]) and proved so later for singularly perturbed models ([13, 14, 15, 24, 25]). For other types of food-chain and food-web chaos, see [26, 11, 27, 28].

However, there is a key difference between chemostat models and food-chain models. The former is "closed" in the sense that the total amount of the substrate is a constant. In contrast, non-chemostat food chains are open in the sense that the total biomass tracked by the models are allowed to vary. Because of this "openness" the growth rates of the interacting species for the latter can vary significantly, allowing a multi-time scale, i.e. singular perturbation analysis for the problem ([29]). The existence of food-chain chaos was indeed obtained by making use of the multi-time property of the food-chain model ([13, 14, 15, 24, 25, 28]).

Constrained by their closeness a singular perturbation approach is not known to apply for chemostat models. However, the geometric analysis of the nullcline surfaces for singularly perturbed systems are equally valid and perhaps more indispensable for general differential equations. In addition, as the nutrient works its way through the food chains from lower trophic levels to higher levels, the growth rates of chemostat species do behave similarly as if they are multi-time scaled: from fast to slow. This gives an empirical as well as a practical justification to treat a chemostat model artificially as an explicit singularly-perturbed system. Our idea is to use the same singular perturbation techniques, which are proved to be very effective for food-chain chaos, to locate first auxiliary singular chaotic attractors, and then to locate real chaotic attractors nearby for the chemostat model by continuing the artificial singular parameter value to its chemostat value. The main theoretical difficulty lies in the continuation problem which remains unsolved. In this paper we will demonstrate chemostat chaos numerically instead.

For any mathematical model of a physical process, simple or complex, proving chaos is always hard. But one strategy is easier to execute. It only requires the existence of a Shilnikov's saddle-focus homoclinic orbit ([30, 31, 32, 33, 34]). More specifically, it says that for a 3-dimensional system of ordinary differential equations $\dot{x} = f(x)$, if there exists a homoclinic orbit $\gamma(t)$ to an equilibrium point p of the Shilnikov type, then the dynamics of the system must be chaotic. The

Shilnikov type equilibrium point is a saddle-focus which without loss of generality by time-reversal if necessary has one negative real eigenvalue $\lambda^s < 0$ and a pair of unstable complex eigenvalues $\lambda^u = \alpha \pm i\beta$ satisfying

$$0 < \mathrm{Re}\lambda^u = \alpha < -\lambda^s, \qquad \mathrm{Im}\lambda^u = \beta > 0. \tag{1}$$

Obviously, such a homoclinic orbit spirals out from the equilibrium along a tangential direction of the 2-dimensional unstable eigenspace and approaches the equilibrium along a tangential direction of the 1-dimensional stable eigenspace. Inside a small neighborhood of the orbit, the dynamics contains at the minimum a Smale's horseshoe, having infinitely many periodic orbits and uncountably many aperiodic orbits.

In fact, the most inclusive version ([33]) for the chaoticness of the dynamics is to say that a sub-dynamics near the orbit is topologically conjugate to a ρ-block shift dynamics $\{\sigma, B_\rho\}$ for any $1 < \rho < -\lambda^s/\mathrm{Re}\lambda^u$. Here B_ρ is a subset of doubly infinite sequences of block symbols $s = \ldots \bar{s}_{-1}.\bar{s}_0\bar{s}_1\bar{s}_2 \ldots$ with $s' = \sigma(s)$ being the same sequence s except that the zero coordinate is shifted one block to the right if $\bar{s}_0$ is a finite block. More specifically, if a symbol $s_i \in \bar{\mathbb{N}}$ is a finite natural number, where $\bar{\mathbb{N}}$ is the compactification of the natural numbers $\mathbb{N}$ at the infinity ∞, then $\bar{s}_i = s_i \cdots s_i$ repeats the symbol s_i many times. If $s_i = \infty$ and $i \geq 0$, then $\bar{s}_i = \infty\infty\cdots$ is the infinite right sequence of the ∞ symbol. If $i < 0$ and $s_i = \infty$, then $\bar{s}_i = \cdots\infty\infty$ is the infinite left sequence of the ∞ symbol. B_ρ is the subset of doubly block symbol sequences for which each block sequence satisfies $s_{i+1} \leq \rho s_i$ for all $i \in \mathbb{Z}$. It inherits the product topology of the doubly infinite product space of the compactified natural numbers, $\bar{\mathbb{N}}^{\mathbb{Z}}$. It is straightforward to show that this system in fact contains infinitely many copies of the shift dynamics on any finite symbols, including infinitely many Smale's horseshoe maps as a special case. It also includes uncountably many orbits from the unstable manifolds that remains inside the neighborhood, corresponding to sequences of the type $\bar{\infty}\bar{s}_n \ldots \bar{s}_{-1}.\bar{s}_0\bar{s}_1\bar{s}_2 \ldots$ with $n \leq -1$ and $s_{i+1} \leq \rho s_i$ for $i \geq n$. Especially, it also includes the sequence $\bar{\infty}.\bar{\infty}$, representing the homoclinic orbit. In precise terms, the result of [33] states that there is a compact subset Λ of any cross-section of a Shilnikov's saddle-focus homoclinic orbit of any sufficiently smooth vector field so that the flow-induced Poincaré return map on Λ is topologically conjugate to the block shift dynamics $\{\sigma, B_\rho\}$ for any ρ satisfying $1 < \rho < -\lambda^s/\mathrm{Re}\lambda^u$.

A singularly perturbed food-chain model was proved to have a parameter region for such homoclinic orbits ([14]). Singularly perturbed systems can also be explicitly constructed to have such orbits ([35, 36]). The goal of this paper is to demonstrate numerically that near the Smith-Waltman parameter value the chemostat model has a Shilnikov's saddle-focus homoclinic orbit, hence demonstrating *in silico* that chaos exits in the sense of the block shift dynamics for the classical 3-dimensional chemostat model.

2. Chemostat Model. Consider a chemostat of a liquid medium of a fixed volume V with a substrate solution continuously pumped in at a constant flow rate r and a substrate concentration c. The well-mixed liquid is also continuously pumped out at the same flow rate r. The substrate can be a type of nutrient or an element essential for life as a common currency, such as carbon, or nitrogen, or iron etc. Let S denote the amount of the substrate that is present in the chemostat and suppose there is a producer feeding on the substrate, a consumer of the producer, and a predator of the consumer with, respectively, X, Y, and Z amounts of the substrate. Examples of such chemostats can be a saltwater or freshwater tank or habitat in which the producer is a phytoplankton, the consumer is a zooplankton grazing on the plant, and the predator is another zooplankton. If we assume the Holling Type II functional form ([37]), then the uptake rate of S per unit of X is

$$\frac{u_1 S}{1 + h_1 u_1 S}$$

where u_1 is the encounter rate, h_1 is the handling time by X. Similarly, the consumption rate of X per unit of Y, and the predation rate of Y per unit of Z are

$$\frac{u_2 X}{1 + h_2 u_2 X}, \quad \frac{u_3 Y}{1 + h_3 u_3 Y},$$

respectively. Assume these species are microorganisms subject to the washout, then the chemostat system is modeled by the following system of equations:

$$\begin{cases} \dot{S} = wN - wS - \dfrac{u_1 S}{1 + h_1 u_1 S} X \\ \dot{X} = \dfrac{u_1 S}{1 + h_1 u_1 S} X - wX - \dfrac{u_2 X}{1 + h_2 u_2 X} Y \\ \dot{Y} = \dfrac{u_2 X}{1 + h_2 u_2 X} Y - wY - \dfrac{u_3 Y}{1 + h_3 u_3 Y} Z \\ \dot{Z} = \dfrac{u_3 Y}{1 + h_3 u_3 Y} Z - wZ \end{cases} \tag{2}$$

where $w = r/V$ denotes the volume-metric flow rate, and $N = cV$ the possible maximal amount of the substrate in the chemostat. Let $K = S + X + Y + Z$ be the total amount of the substrate in the system. Then by summing up all the equations above, K satisfies

$$\dot{K} = wN - wK$$

which in turn implies $K(t)$ converges exponentially fast to the constant N. Therefore, to study the longtime behavior of the chemostat we only need to assume the dynamics of the system is already on the hyperplane

$$N = S + X + Y + Z$$

which reduces the dimension of the model by one to becoming

$$\begin{cases} \dot{X} = \dfrac{u_1(N-X-Y-Z)}{1+h_1u_1(N-X-Y-Z)}X - wX - \dfrac{u_2X}{1+h_2u_2X}Y \\ \dot{Y} = \dfrac{u_2X}{1+h_2u_2X}Y - wY - \dfrac{u_3Y}{1+h_3u_3Y}Z \\ \dot{Z} = \dfrac{u_3Y}{1+h_3u_3Y}Z - wZ. \end{cases} \tag{3}$$

142 By the following change of variables

$$\begin{cases} t := wt, \quad x = \dfrac{X}{N}, \quad y = \dfrac{Y}{N}, \quad z = \dfrac{Z}{N} \\ a_1 = \dfrac{1}{u_1h_1N}, \quad a_2 = \dfrac{1}{u_2h_2N}, \quad a_3 = \dfrac{1}{u_3h_3N} \\ m_1 = \dfrac{1}{h_1w}, \quad m_2 = \dfrac{1}{h_2w}, \quad m_3 = \dfrac{1}{h_3w} \end{cases} \tag{4}$$

the dimensional model is transformed to this dimensionless form

$$\begin{cases} \dot{x} = x\left(\dfrac{m_1(1-x-y-z)}{a_1+(1-x-y-z)} - 1 - \dfrac{m_2}{a_2+x}y\right) \\ \dot{y} = y\left(\dfrac{m_2x}{a_2+x} - 1 - \dfrac{m_3}{a_3+y}z\right) \\ \dot{z} = z\left(\dfrac{m_3y}{a_3+y} - 1\right) \end{cases} \tag{5}$$

144 In this way, the uptake, consumption, and predation rates, $\frac{m_iP}{a_i+P}$, are of the Monod form ([1]) with m_i being the dimensionless maximal rates and a_i the half-saturation constants. Because of mass
146 conservation with $N-X-Y-Z=S\geq 0$ (correspondingly, $1-x-y-z\geq 0$), the effective phase space for the variables is inside the simplex

$$\Delta = \{(x,y,z) : x+y+z \leq 1,\ x\geq 0,\ y\geq 0,\ z\geq 0\}$$

148 in the first octant as all population densities are non-negative numbers. Note that each coordinate plane is invariant for the model representing the extinction of a species. This is the chemostat
150 model considered in [4] for the Smith-Waltman attractor.

A singularly perturbed system of equations is one for which there is a small positive parameter
152 multiplied to either the left hand or right hand side of some equation. Such a small parameter, when multiplied to the left hand side, makes the corresponding variable to change fast relative
154 to other variables, which in turn makes the system a multi-time scaled process. Although the dimensionless form of the chemostat model above is not explicitly a singular-perturbation form,

the multi-time scale property is inherent of the chemostat process because as the nutrient element works its way up the food chain, its assimilation by a higher trophic consumer becomes slower. It is very similar to a typical food chain model for which the plant, for example, at the bottom of the chain regenerates fast comparing to the herbivores which feed on the plant.

Mathematically, it is usually easier to study singular perturbation problems. One useful feature is the fact that many qualitative information remain the same for all values of the singular parameter because the sign of the right hand side of each equation does not vary with the singular parameter. As an auxiliary means we introduce one artificial singular parameter $0 < \varepsilon \ll 1$ for the producer X, making the system explicitly a singularly perturbed one:

$$\begin{cases} \varepsilon \dot{x} = x\left(\dfrac{m_1(1-x-y-z)}{a_1+(1-x-y-z)} - 1 - \dfrac{m_2}{a_2+x}y\right) := xf(x,y,z) \\ \dot{y} = y\left(\dfrac{m_2 x}{a_2+x} - 1 - \dfrac{m_3}{a_3+y}z\right) := yg(x,y,z) \\ \dot{z} = z\left(\dfrac{m_3 y}{a_3+y} - 1\right) := zh(y) \end{cases} \tag{6}$$

This system will be referred to as the auxiliary model, or the singularly perturbed model. Results obtained for the singularly perturbed model will be used to guide our search for Shilnikov's saddle-focus homoclinic orbit for the original chemostat model which can be considered as the continuation of the auxiliary system to the native value $\varepsilon = 1$. The main advantage of using singular perturbations lies in its dimension reduction for analysis for which lower dimensional subsystems tend to be simpler. By piecing together such lower dimensional structures and properties one can build a fairly accurate big picture for the whole system using the limiting structure at $\varepsilon = 0$ as an approximation.

3. Singular Perturbation Analysis. Our approach in this paper is geometric. It is to analyze the vector field of the equations by the configurations of the variables nullclines in order to obtain good approximations of their solutions for small value of the singular parameter. An approximating orbit is a so-called singular orbit at the limiting value $\varepsilon = 0$ that is the concatenation of some fast and slow orbits connecting between or trekking on some nullclines of the equations.

Fast Producer Dynamics: By rescaling the time $\tau = t/\varepsilon$ for Eq.(6), and setting the singular parameter at its singular value, $\varepsilon = 0$, we obtain the fast subsystem

$$x' = xf(x,y,z), \qquad y' = 0, \qquad z' = 0.$$

It is a one-dimensional system with y, z being frozen as parameters. This system can be completely understood by a simple phase line analysis. Specifically, the dynamics is determined by its equilibrium points and the signs of the vector field off the equilibrium points. In fact, in the orig-

inal xyz-phase space, the set of the x-equilibrium points consists of the trivial coordinate plane $x = 0$, corresponding the extinction state of the producer, and the nontrivial nullcline surface $f(x, y, z) = 0$. This surface usually consists of two branches: the capacity branch and the persistent threshold branch. These branches can be understood qualitatively by biological arguments.

Suppose the consumer and the predator are absent, i.e. y and z are kept at $y = z = 0$, then the producer dynamics $x' = xf(x, 0, 0)$ is the kind of logistic, with the capacity equilibrium point $\bar{x} > 0$ solved from $f(\bar{x}, 0, 0) = 0$ as

$$\bar{x} = 1 - \frac{a_1}{m_1 - 1}.$$

Because of the conservation of mass, we must have $0 \leq x \leq 1$ which implies that

$$m_1 = \frac{1}{h_1 w} > 1.$$

That is, the handing rate, $1/h_1$, of the producer must be greater than the volume-metric washout rate, w, in order for it to establish the capacity equilibrium state. Moreover, since

$$f(x, 0, 0) = \frac{m_1(1 - x)}{a_1 + (1 - x)} - 1 < 0 \qquad \text{if and only if} \qquad x > \bar{x}$$

as determined by the one-point test at $x = 1$, we know that $\bar{x}$ is indeed a capacity equilibrium. This capacity equilibrium point will continue for non-zero y and z. More specifically, for each fixed z value, the capacity branch as y changes can be easily understood. In fact, as the strength of the predation increases by y on x, the x-capacity equilibrium must decrease from the largest capacity $\bar{x}$. That is, on any z-section, the function $\bar{x}$ is a decreasing function of y.

Two scenarios exists. As y increases, the x-capacity branch of the nullcline surface $f = 0$ decrease to the extinction branch $x = 0$ at some predatory strength of y. The second scenario is, as y increases above a certain value $\bar{y}_f$, the x-capacity equilibrium ceases to exist beyond a nontrivial value $\bar{x}_f > 0$. In other words, for $y < \bar{y}_f$, there exist the x-capacity equilibrium $\bar{x}$, but for $y > \bar{y}_f$, it induces a population crash on the producer x: all phase lines converge to the extinction state $x = 0$.

As for the persistent or survival threshold branch, we know at $y = z = 0$, the persistent equilibrium branch is the extinction state $x = 0$, namely, for any trajectory starting with positive x converges to the capacity equilibrium state $\bar{x}$, i.e. the equilibrium state $x = 0$ is unstable. As the predation increase in y, $x = 0$ may continue to have the same repelling property. In the case of the existence of the crash capacity $\bar{x}_f > 0$ and $\bar{y}_f > 0$, there must be a predation strength smaller than the crashing strength so that not all non-zero initial values of x will develop to approach the capacity state $\bar{x}$. Denote this critical value by $y = y_{trn}$ with the subscript standing for 'transcritical'

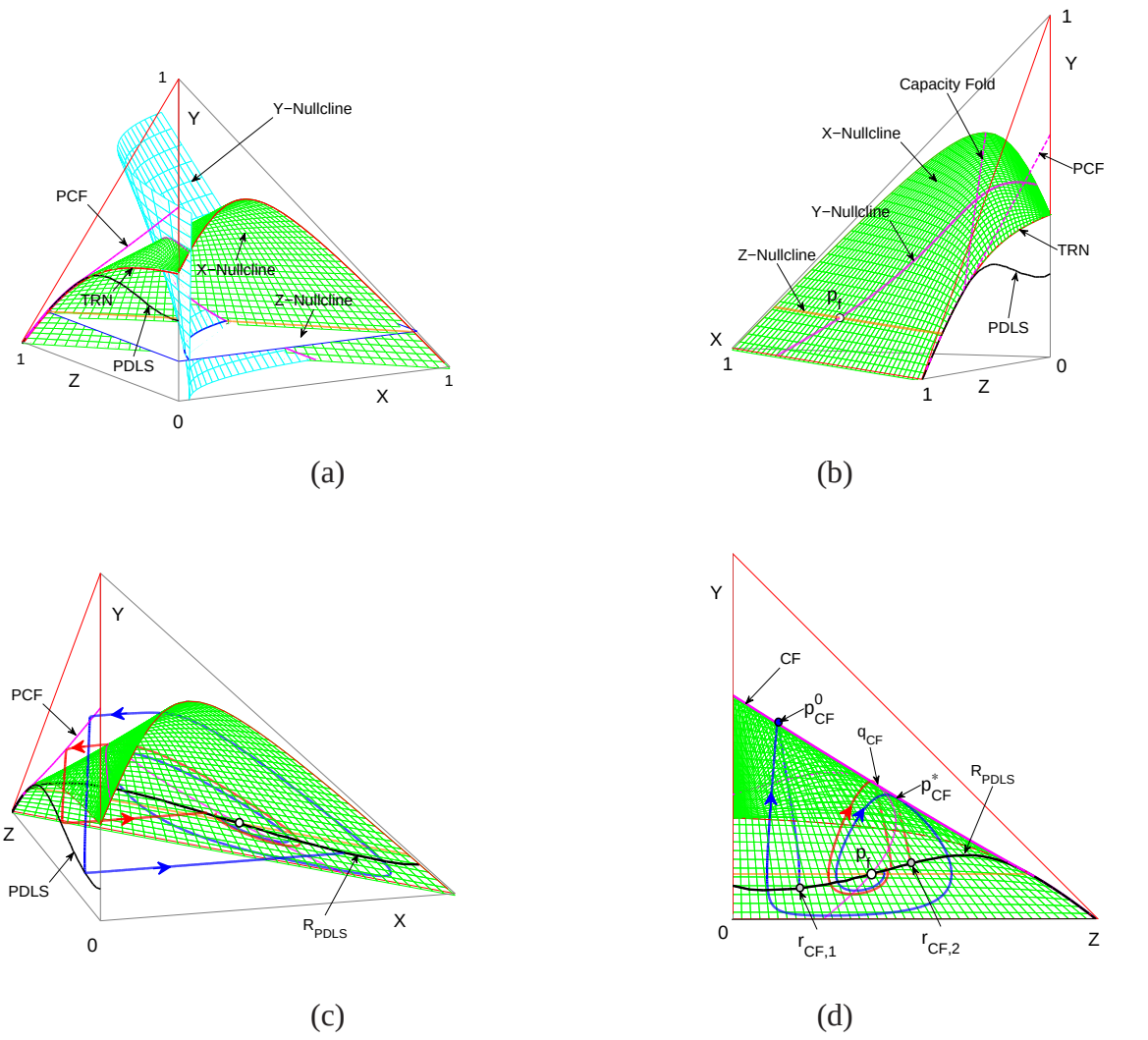

Figure 2: (a) Typical nullcline surfaces for the variables. (b) The same plot as (a) without the y-nullcline and z-nullcline surfaces but with their intersections with the x-nullcline surface. The curve PCF is the projection of the capacity fold to the yz-plane along the fast x-direction. It is where the population crash lands in y and z from the crash points on the capacity branch and the threshold branch. TRN is the set of the transcritical points for the x-equation, and PDLS is the set of Pontryagin's Delay of Lost Stability. (c) Singular orbits are concatenations of fast orbits between the attracting branches of the slow manifold of the x-equation and slow orbits on the extinction branch and on the capacity branch. Crashing fast orbits from the capacity fold can only rebound at the PDLS points. (d) Phase portrait of the slow yz-system on the capacity branch and the extinction branch of the slow manifold. For $\varepsilon = 0$, the interval $[r_{CF,1}, r_{CF,2}]$ on the returning PDLS curve, R_{PDLS}, defines the range of the unstable manifold of the equilibrium point p_f. A singular homoclinic orbit exists if and only if the $[r_{CF,1}, r_{CF,2}]$ segment of R_{PDLS} contains p_f.

to be explained shortly. This means, for any immediate predation strength greater than y_{trn}, there exist a nontrivial persistent equilibrium $x = \underline{x} > 0$ so that for initial population density x_0 greater

than $\underline{x} > 0$ the population grows and converges to the capacity state $\bar{x}$, and otherwise, if $x_0 < \underline{x}$, the population decreases to the extinction state. That is, the $\underline{x}$ is the threshold for persistence: above it the population persists and below it the population goes extinction. Moreover, as a function of the y value, this threshold branch $\underline{x}$ increases, the higher the predation, the greater threshold required for persistence. As solutions to the nullcline equation $f(x, y, z) = 0$, for each fixed z, the survival threshold branch and the capacity branch approach each other as y increases, until they meet at the crash point $x = \bar{x}_f$ and $y = \bar{y}_f$. That is, for each fixed z, the point $(\bar{x}_f, \bar{y}_f)$ is a fold point of the nullcline surface $f(x, y, z) = 0$. Last, for each point z, $x = 0, y = y_{trn}$ is where the threshold branch $\underline{x}$ meets the extinction branch $x = 0$. Since both $x = 0$ and $f = 0$ are nullclines of the x-equation, their intersection points are the so-called transcritical bifurcation points, and hence the notation. For illustrations of the x-nullcline, the capacity and the threshold branches, the capacity fold, and the transcritical curve, see Fig.2.

Algebraically, the nullcline equation $f(x, y, z) = 0$ can be solved by expressing one variable as a function of the other two. In particular, x or y can be solved as a root to a quadratic equation, but z can be solved as a simpler, linear equation in z. The transcritial curve $y = y_{trn},\ x = 0$ can be solved from $f(0, y, z) = 0$ for which z can be solved from a simpler linear equation in z. The crash-fold curve can be solved from the pair of equations:

$$f(x, y, z) = 0, \qquad f_x(x, y, z) = 0$$

because for each z the nullcline curve $f(x, y, z) = 0$ reaches a global maximum in y at the crash-fold point $(\bar{x}_f, \bar{y}_f)$ at which $dy/dx = -f_x/f_y = 0$. As a result, all these curves can be solved explicitly for plotting.

As for the singularly perturbed equations, the x-nullcline branches are also referred to as the slow manifolds. Moreover, the capacity branch of the slow manifold is attracting, the extinction branch above the transcritical curve y_{trn} is also attracting, but the threshold branch and the extinction branch below the transcritical curve are repelling. Furthermore, for every non-equilibrium initial point below the slow manifold $f = 0$, the solution converges to the capacity branch. For every non-equilibrium initial point above it, the solution converges either to the capacity branch or to the extinction branch depending on the initial state. If the initial consumer population y is below the crashing value $\bar{y}_f$ and x is above its capacity equilibrium $\bar{x}$, then the solution converges to the x-capacity branch, and for all other initials, the solutions converge to the extinction branch.

Two more comments are in order for the slow manifold. We note that the x-nullcline $f = 0$ is always inside the definition simplex Δ because of the terms $-1 - m_2 y/(a_2 + x)$. That is, all the discussions above remain relevant to the chemostat dynamics. Second, the z-section curves of the x-nullcline surface $f = 0$ is nested as z increases. That is, the crash fold y value $\bar{y}_f$ is decreasing in z as the larger the z a smaller y is sufficient to crash the x population as the presence of z leaves fewer resource for x. Also, the higher the z, the lower in y for the capacity branch for a same x

value, implying the z-sectional x-capacity curve is nested inward. Similarly, the higher the z the lower the persistent threshold y_{trn} value as it takes a lower predation pressure by y on x for the x species to develop the survival threshold.

Slow Consumer-Predator Dynamics: When setting $\varepsilon = 0$ in Eq.(6), we obtain the slow dynamics on the slow manifolds:

$$0 = xf(x, y, z), \qquad \frac{dy}{dt} = yg(x, y, z), \qquad \frac{dz}{dt} = zh(y).$$

On either the extinction branch $x = 0$ or the capacity branch $f = 0, x = \bar{x}_f$, the dynamics is planar, and therefore can be completely described geometrically. On the extinction branch $x = 0$, the dynamics is simple: without the producer, the y population is strictly decreasing (because $dy/dt = yg(0, y, z) = y(-1 - m_3/(a_3 + z)) < 0$). The z population is slightly less so: If the population is above the z-nullcline $h(y) = 0$, which solves to be $y = y_{zncl} = a_3/(m_3 - 1)$, the predator can still manage to grow for awhile, but starts to decline as soon as it crosses the nullcline $y = y_{zncl}$, and then both go towards extinction. Because y is strictly decreasing on $x = 0$, it will be used later as a change of variable for the time variable t.

On the x-capacity slow manifold, the reduced slow dynamics is a little more involved, but not too much so. In fact, a similar capacity-threshold type of argument applies because the reduced dynamics for y and z is just another predator-prey system except for the constraint that the interaction must be confined by the x-capacity fold line as a boundary on the x-capacity branch of the slow manifold. Analytically, one can solve x from $f(x, y, z) = 0$ as the solution of a quadratic equation, substitute the x-capacity branch solution into the right-hand side of the y equation to obtain the reduced yz-slow system. For which a phase plane analysis can be carried out, in particular, at the equilibrium point. Alternatively, here is a more geometrical and empirical analysis of the reduced 2-dimensional predator-prey system. Specifically, for each fixed z value (imagining an experimenter can hold the z species constant), then the dynamics is only one-dimensional in y, determined entirely by its equilibrium states $g = 0$ and the sign of g. In fact, the intersection of $g = 0$ and $f = 0,\ x = \bar{x}_f$ is the nontrivial equilibrium points of the y-equation, for which it can be divided up into its capacity branch and its survival threshold branch as z sweeps from low to high values, see Fig.2(d). For the parameter regions of interest, it has the survival threshold branch, which increases in y as z increases, and is unstable for the reduced y-equation. This threshold may continue to hit the x-slow manifold's capacity fold or merge with a capacity fold point for the y species. That is, in the latter case, the y-nullcline on the x-capacity slow manifold is a unimodal curve, and the decreasing branch with increasing z is the stable y-capacity equilibrium states. So the y-nullcline on the x-capacity slow manifold is either increasing or has one interior maximum corresponding the y crash fold by z. In any case, denote the intersection point of the y-nullcline on the x-capacity slow manifold with the x-capacity fold by q_{CF} as shown in Fig.2(d). As for the z-nullcline on the slow manifold, it cannot be simpler because it is only a line parallel with

the z-axis $y = y_{zncl}$. As a result, the reduced slow dynamics on the x-capacity manifold is completely determined by the y-nullcline and the z-nullcline. That is, inside the y-nullcline, y always increases, either hitting the x-crash fold in finite time or crossing the y-capacity branch vertical to the y-axis. Outside the y-nullcline, y decreases because the predation pressure from z is too high. As for the z, above its nullcline $y = y_{zncl}$, z increases as there are sufficiently many y to sustain its growth, and below it z declines.

As the z-nullcline is a straight line, perpendicular to the y-axis, it can intersect the y-nullcline only at one point, denoted by p_f when existing, which is the unique coexisting population equilibrium of the full system. We will further consider the parameter regions for which the z-nullcline is through the y-species' survival threshold branch of the y-nullcline. This can be achieved by lowering the z-nullcline $y = y_{zncl} = a_3/(m_3 - 1)$ which can be done by either decreasing a_3 or increasing m_3.

Since it lies on the unstable branch of the y-nullcline, the equilibrium point p_f is always unstable. In fact, it is always a source. More specifically, let

$$\begin{cases} \dot{u} = au - bv \\ \dot{v} = cu \end{cases} \tag{7}$$

denote the linearization of the reduced yz-system at the equilibrium point p_f. Then, it only takes a qualitative argument to know that the linearized u-nullcline $au - bv = 0$ is tangent to the y-nullcline at the equilibrium point and so is for the v-nullcline $u = 0$ to the z-nullcline. Because u, v mirror the roles of the consumer y and the predator z,respectively, the linearization coefficients b, c must be positive. In addition, since the equilibrium point p_f is on the y-survival threshold of the y-nullcline, the linearization coefficient a must be positive as well. As a result, the eigenvalues of the reduced slow system at the equilibrium point are

$$\lambda = \frac{a \pm \sqrt{a^2 - 4bc}}{2},$$

which are either all positive or a pair of complex numbers with positive real part. For the equilibrium point to be an unstable focus point with complex eigenvalues, we only need the predator z to be considerably strong as the linearization coefficients b and c are strongly depending on the efficiency of the predator which in turn can be achieved by increasing m_3 and decreasing a_3. As a passing remark, if the equilibrium point is on the y-capacity branch for which the linearization coefficient a must be negative, then both eigenvalues must have a negative real part, confirming the stability of the equilibrium solution.

One special point for the reduced slow dynamics stands out that will be used later. It is the point on the x-crash fold curve, which defines the boundary of the reduced yz-slow vector field. Since the x-crash fold is decreasing in y as z increases, and since the slow vector field is perpendicular

to the y-direction, pointing outward from the fold at the fold point q_{CF} when above the z-nullcline, and since the vector field is perpendicular to z-nullcline, there must be a point by continuity on the x-crash fold boundary, denoted by p^*_{CF}, at which the vector field is tangent to the fold boundary. See Fig.2(d). As we will see below, this point is instrumental in defining the range of the global unstable manifold of the equilibrium point p_f.

Pontryagin's Delay of Lost Stability: If we follow the slow orbit on the x-capacity manifold staring at the tangent fold point p^*_{CF}, we will eventually hit the capacity fold at a point denoted by p^0_{CF}, a boundary of the capacity manifold on which the reduced slow equations are defined. If we follow the fast x-equation, the fast orbit will bring it to a point on the extinction surface $x = 0$. In fact, the fast orbit starting from any point of the x-capacity fold converges to a point on the extinction surface. The set of all these limiting points is referred to as the projection of the capacity fold (PCF as shown in Fig.2). The next concatenation of such an orbit is to follow the slow orbit on the extinction surface, that must cross the transcritical curve $y = y_{trn}$ to enter the unstable branch of the extinction surface. By the theory of singular perturbation, this slow orbit must not go down indefinitely in y and z. Instead, somewhere in the $x = 0$ slow manifold, the fast dynamics arises and takes over, concatenating a fast orbit toward the x-capacity surface again. This phenomenon is referred to as the Pontryagin's delay of lost stability (PDLS) and here below is how the points in (y, z) on the PDLS set is computed.

It is found by first considering orbits for the perturbed full system with $0 < \varepsilon \ll 1$ and then taking the limit $\varepsilon \to 0$ to find the PDLS points. More specifically, let $p_{CF} = (x_0, y_0, z_0)$ be a crash fold point with $x_0 > 0$ and let $0 < \delta < \min\{x_0, a_2/(m_2 - 1)\}$ be a small constant and consider the plane $x = \delta$. Then consider the solution of the singularly perturbed equations, $\phi^\varepsilon(t) = (x^\varepsilon(t), y^\varepsilon(t), z^\varepsilon(t))$, with the initial point $\phi^\varepsilon(0) = (\delta, y_0, z_0)$. By a phase space analysis, this orbit must decreasing in x and y first because the initial point is above the x-survival surface and below the y-nullcline surface $z = (\frac{m_2 x}{a_2+x} - 1)\frac{a_3+y}{m_3}$ as $z \geq 0$ if and only if $x \geq a_2/(m_2 - 1)$. At sometime later the orbit crosses the x-survival threshold surface on the x-nullcline. Afterward the orbit must increase in x because it is below the x-capacity surface with y keeping decreasing. At a finite time later, $t = \bar{t}$, the orbit hits the plane $x = \delta$ again, this time below the x-survival surface. The time $\bar{t}$ depends on ε obviously given by $x^\varepsilon(\bar{t}) = \delta$. In any case, it is important to note that the starting and ending points for the orbit over the time interval $[0, \bar{t}]$ are both on the same plane $x = \delta$. Also, because the plane $x = \delta$ lies always below the y-nullcline, we must have $g < 0$ on the orbit in the same time interval. As a result, the variable y along this orbit is always decreasing and thus can be used as a change of variable to substitute out the time variable as $dt = dy/(yg)$.

Thus the following identities must hold

$$\begin{aligned} 0 &= \varepsilon(\ln x^{\varepsilon}(\bar{t}) - \ln x^{\varepsilon}(0)) \\ &= \varepsilon \int_0^{\bar{t}} \frac{1}{x^{\varepsilon}(t)} \frac{dx^{\varepsilon}}{dt} dt \\ &= \int_0^{t} f(x^{\varepsilon}(t), y^{\varepsilon}(t), z^{\varepsilon}(t)) dt \\ &= \int_{y_0}^{b(\varepsilon)} \frac{f(\tilde{x}^{\varepsilon}(y), y, \tilde{z}^{\varepsilon}(y))}{y g(\tilde{x}^{\varepsilon}(y), y, \tilde{z}^{\varepsilon}(y))} dy \end{aligned}$$

where $b(\varepsilon) = y^{\varepsilon}(\bar{t}), \tilde{x}^{\varepsilon}(y) = x^{\varepsilon}(t), \tilde{z}^{\varepsilon}(y) = z^{\varepsilon}(t)$ with t being the function of y by the change of variables $y = y^{\varepsilon}(t)$ which is strictly decreasing in t. Take the limit to the singular value $\varepsilon \to 0$, assume the limit of $b(\varepsilon)$ exists and denote it by $\lim_{\varepsilon \to 0} b(\varepsilon) = y_{pdls}$. Then y_{pdls} is a function of the initial (y_0, z_0) but not $x_0 = \delta$ as any different value of δ nearby results in the same fast orbit through (x_0, y_0, z_0) perpendicular to the yz-plane and the same slow orbit on the extinction manifold for Eq.(6) with $\varepsilon = 0$ and $x = 0$. The fast orbit has zero contribution to the limit integral above because it is perpendicular to the integration y variable. As a result the so-called PDLS point $y_{pdls}(y_0, z_0)$ is determined from the equation below:

$$\int_{y_0}^{y_{pdls}} \frac{f(0, y, \tilde{z}(y))}{y g(0, y, \tilde{z}(y))} dy = 0 \tag{8}$$

where $\tilde{z}(y) = z(t)$ denotes the $x = 0$ slow solution $(y(t), z(t))$ with the initial point (y_0, z_0) from the projection of the x-capacity fold for which the time variable t is changed to y through $y = y(t)$ because the latter is strictly decreasing on the invariant plane $x = 0$. We also note that the PDLS point y_{pdls} must lie below the transcritical curve $y = y_{trn}$ because above the curve the integrant above is of one sign and below it it is of the opposite sign. The resulting PDLS curve corresponding to the x-capacity fold is denoted by PDLS in Fig.2(c).

Singular Shilnikov Orbit: Every PDLS point will be projected by the x-fast orbit to a capacity point on the x-slow manifold. Denote the set of the projected PDLS points by R_{PDLS} as shown in Fig.2(c,d). We will consider only those parameters regions for which the tangential crash-fold point p^*_{CF} lies above the returning R_{PDLS} curve as shown in Fig.2(d). Then the x-fast orbit from the tangential point p^*_{CF} can first go to the extinction branch, then down to its PDLS point, and finally return to the x-capacity slow manifold on the curve R_{PDLS}. Denote this returning point by $r_{CF,2}$ as shown. Denote also the returning point of the corresponding concatenation of singular orbits from p^0_{CF} by $r_{CF,1}$. Then we can conclude that the local unstable manifold W^u_{loc} of the equilibrium point p_f returns only to the interval segment between $r_{CF,1}$ and $r_{CF,2}$ on R_{PDLS} at the singular limit $\varepsilon = 0$. As a result, we have the following statement.

Theorem 1 *For the singularly perturbed model Eq.(6), a singular Shilnikov saddle-focus homo-*

clinic orbit exits if p_f is inside the R_{PDLS} interval segment between $r_{CF,1}$ and $r_{CF,2}$ for which the equilibrium point p_f when restricted to the slow manifold is an unstable focus point and p^*_{CF} is on the x-crash fold and lies above the R_{PDLS} curve.

We note that the resulting homoclinic orbit is of the Shilnikov kind because the stable eigenvalue of the equilibrium point p_f at the singular value is $-\infty$ with the x-direction being the stable eigenvector, always satisfying the eigenvalue condition (1) for Shilnikov's saddle-focus homoclinic orbit.

The strategic importance of this result lies in the geometric configuration for the singular Shilnikov's orbit which we use as a guide to locate first the parameter regions for such configuration, and then through continuation of the auxiliary singular parameter ε to its native value $\varepsilon = 1$ to locate the parameter values at which a Shilnikov's saddle-focus homoclinic orbit exits for the original chemostat model. Proving the theorem for the auxiliary singularly perturbed model of the chemostat equations for specific parameter regions is to match the singular global unstable manifold R_{PDLS} to the equilibrium point for the parameter regions. It essentially requires a shooting type of argument in theory and in numerics. The key theoretical difficulty lies in the computation of the PDLS curve analytically, not only as a function of the x-capacity fold curve but also of the parameters. In what follows we will only attempt to demonstrate the theorem numerically by a shooting algorithm.

4. Numerical Shooting Method. On the nontrivial x-nullcline $f = 0$, we find the nontrivial y-nullcline intersection curve $f = 0, g = 0$. This curve can be obtained this way. First, solve z as a function of x, y from $g = 0$, substitute it into $f = 0$ to solve y from an eventual quadratic equation as a function of x, which in turns is back substituted to express z as a function of x. The nontrivial z-nullcline intersection curve with the nontrivial x-nullcline is much easier to find. The z-nullcline $h = 0$ is solved as a y constant $\bar{y} = a_3/(m_3 - 1)$, which is substituted into $f = 0$ to solve z as a function of x. As a result, the nontrivial equilibrium point with all non-vanishing populations can be numerically solved as the intersection of the these two curves. Denote the equilibrium point as $p_f = (x_f, y_f, z_f)$ and refer to it sometimes as the coexisting equilibrium point. Numerically, we used a discretization step size about the order of 10^{-8} for the x variable for these two curves and expect the same accuracy for the equilibrium point.

For the linearization of the vector field at the equilibrium point,

$$J(\bar{p}) = \begin{bmatrix} \bar{x}f_x & \bar{x}f_y & \bar{x}f_z \\ \bar{y}g_x & \bar{y}g_y & \bar{y}g_z \\ 0 & \bar{z}h_y & 0 \end{bmatrix}$$

we use the first order discretization scheme for the partial derivatives with an increment of 10^{-10}. The corresponding stable and unstable eigenvector sets are denoted as λ_s and λ_u respectively. For the parameter values considered, the equilibrium point p_f is a saddle focus with $\lambda_s < 0$ and

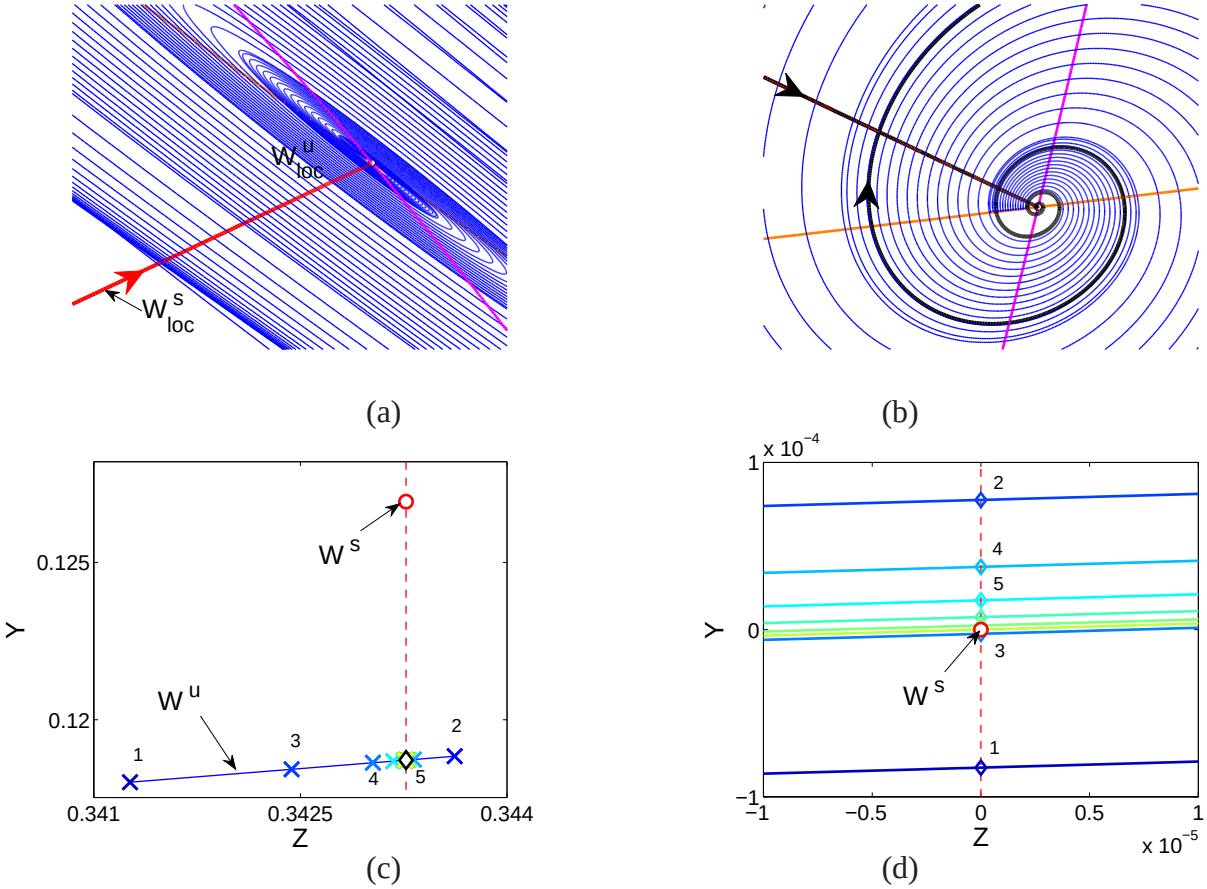

Figure 3: (a) The local stable and unstable manifolds of the coexisting equilibrium point is approximated by the linearization of the vector field at the equilibrium point. It is done in a δ-neighborhood of the equilibrium point with $\delta \sim 10^{-4}$. (b) A view of the local unstable manifold, for which the orbit in black shows a Shilnikov's orbit, which starts at a distance of order 10^{-4} from the equilibrium point and returns at a distance of order 10^{-6}. (c) For each parameter a_2, the bisection search routine for the initial of the target point p^u (diamond) takes place along the z-direction of W^u, around the vertical line $z = z^s$ through W^s. The numbers show the bisection steps in sequence to locate the unstable manifold orbit whose return is closet to the vertical line. (d) The bisection search routine for the a_2 parameter starts with two values whose corresponding cross-sections W^u lie above the stable manifold point W^s for one and below for the other. The numbers show the bisection steps to locate the parameter value whose W^u crosses W^s, e.g. the unstable manifold orbit (diamond) on the vertical line meets the stable manifold (circle). (Each W^s is translocated to $(0, 0)$ for a common reference for all parameters.)

$\mathrm{Re}\lambda_u > 0$ and $\mathrm{Im}\lambda_u = \pm\beta \neq 0$. Also, it is of the Shilnikov kind with $-\lambda_s > \mathrm{Re}\lambda_u$. The stable eigenvector space E^s and unstable eigenvector space E^u can also be obtained numerically, and they are used to approximate the local stable and local unstable manifolds, $W^s_{\mathrm{loc}}, W^u_{\mathrm{loc}}$, respectively. All unstable manifold orbits are originated from an Euclidean δ-neighborhood of the equilibrium point with $\delta \sim 10^{-4}$. See Fig.3(a,b). Because the tangent eigenspaces approximate the stable and

unstable manifolds to higher orders, the complementary direction errors between the eigenspaces and the manifolds are of order at least $\delta^2 \sim 10^{-8}$.

To guarantee no region of the local unstable manifold is overlooked numerically, we start at any initial point, a, from E^u, to the left side of the equilibrium point and on the z-nullcline surface $y = y_{zncl}$. We use the z-nullcline surface as a cross-section and find the first return, b, of a to its left side since p_f is an outward unstable spiral. This pair is on a full expanding spiral on the local unstable manifold $W^u_{\rm loc}$. We then partition the interval between a and b on E^u and $y = y_{zncl}$ into a set of many points, and use them as the initial points of a family of unstable orbits. In this way, the local unstable manifold $W^u_{\rm loc}$ is completely bounded by this family of orbits when integrated backwards. And, when integrated forward, this family of orbits defines the global unstable manifold. See Fig.3(b).

The plane for shooting is defined to be this plane inside the simplex Δ:

$$\Sigma := \{(x, y, z) | 2x + y + z = 1,\ x \geq 0, y \geq 0, z \geq 0\}$$

going through these axis points: $(1/2, 0, 0),\ (0, 1, 0)$ and $(0, 0, 1)$. Take any point on the stable eigenspace E^s inside the δ-neighborhood, integrate backward to intersect the plane Σ. Denote the intersection of the global stable manifold with the plane by $W^s = \{(x^s, y^s, z^s)\}$. It is typically a point. Similarly, integrate the family of local unstable manifold orbits forward to intersect the plane, and denote it by W^u. The intersection is the first returning intersection in the sense that the orbit hits the plane from behind and toward the capacity branch of the x-nullcline. It is typically a curve. The goal of the shooting algorithm is to find the parameter values of the system so that the stable and unstable manifold intersect:

$$W^s \in W^u. \tag{9}$$

Finding homoclinic orbits satisfying the above condition takes two searching routines, both are iterative bisections of intervals. The first is a bisection search on the unstable manifold W^u on the plane Σ. It is to find the initial point on the local unstable manifold $W^u_{\rm loc}$ whose returning point on W^u is the intersection of W^u with the line $z = z^s$ through the stable manifold point $W^s = \{(x^s, y^s, z^s)\}$. Denote this shooting target point on W^u by $p^u = (x^u, y^u, z^u)$. When a parameter permits, this is done by first locate two points on W^u, referred to as p_1, p_2, each is on one side of the target p^u as shown in Fig.3(c). Since these two points are generated from two points from the local unstable manifold $W^u_{\rm loc}$ on the line $y = y_{zncl}$ and to the left side of the equilibrium point, we then use the middle point of the initials to create another point on W^u, referred to as p_3. For the right parameter value, p_3 is between p_1 and p_2. Depending on which side of the target point p^u the p_3 point is, a smaller interval is found to contain the target p^u, and another iteration follows to find the next approximation to the target p^u, and so on.

Not all parameters of a system can permit this bisection search. The condition for this routine to run is the existence of points p_1, p_2 on W^u that straddle p^u, i.e.

$$z_1 \leq z^u \leq z_2 \qquad \text{or} \qquad z_2 \leq z^u \leq z_1 \tag{10}$$

where z_i is the z-coordinate of $p_i \in W^u$.

For this bisection search, we use 25 iterative bisection steps to approximate the target p^u. Denote the last point by $\tilde{p}$. Obviously, if $\tilde{p} = p^s$ within a preset tolerance, then a numerical homoclinic orbit is found and the corresponding initial point from W^u_{loc} is the sought-after homoclinic point. The reason to carry out this many bisection steps is because, assuming each search interval is reduced by half, the end search point should be within a distance of $2^{-25} \sim 3 \times 10^{-8}$ of the exact target.

Since homoclinic orbit is a co-dimension one bifurcation phenomenon, for almost all parameter values, there is a gap between $\tilde{p}$ and p^s. The second bisection search routine is carried out for a carefully chosen parameter to close this gap. We will explain why a_2 parameter is chosen for this search shortly. For now let us assume it is the case. Then the bisection search for the homoclinic parameter for which condition (9) holds works similarly as the first bisection search for $\tilde{p}$. More specifically, assume two parameter values of a_2 are found so that one $\tilde{p}$ is above its W^s on its line $z = z^s$ and another $\tilde{p}$ is below its W^s on its line $z = z^s$. We then generate the next parameter value as the middle point of the first two and find its $\tilde{p}$ by the first bisection search routine, and so on, see Fig.3(d).

Similar to the bisection condition for $\tilde{p}$ above, the bisection condition for the searching parameter a_2 is the existence of two $\tilde{p}$ of two parameter values that bound W^s. That is, when W^s is translocated to $(0, 0)$ for all parameters, there are two parameter values whose corresponding $\tilde{p}$ points are denoted by $\tilde{p}_1, \tilde{p}_2$ so that

$$\tilde{y}_1 \leq 0 \leq \tilde{y}_2 \qquad \text{or} \qquad \tilde{y}_2 \leq 0 \leq \tilde{y}_1 \tag{11}$$

where $\tilde{y}_i$ is the y-coordinate of $\tilde{p}_i$, relative to their own W^s.

We can either run this hierarchy search routine for a finite number of steps or set it to terminate if a preset precision is reached between $\tilde{p}$ and W^s. The maximal number of steps is set to be 25 and the stoppage search error is set to be 10^{-6}. As a result, if the shooting algorithm converges, the number of steps taken should not exceed the program maximum 25 as $2^{-25} \sim 3 \times 10^{-8}$. Also the numerical homoclinic orbit found is expected to return to a small neighborhood of the equilibrium point of radius about 10^{-4}, as a conservative ballpark estimate. We will denote it by E_e the shortest Euclidean distance of the unstable manifold orbit through the last $\tilde{p}$ that first enters the δ-neighborhood of the equilibrium point. This measures how much the numerical homoclinic orbit misses the target equilibrium point. When the shooting algorithm converges, we expect E_e to

be no greater than 10^{-4}.

If one of the conditions (10, 11) does not hold, the shooting algorithm will not converge to find a homoclinic orbit. The algorithm will also stop working if the model becomes too stiff for the ODE solvers employed for the searching routines. Since our singular perturbation analysis will guide us to a parameter range for which the second search condition (11) hold initially, for all searches that we carried out but failed to converge it was because the first search condition (10) fails or the singular parameter ε is too small for the ODE solver used.

Because for sufficiently small ε the global return W^u of the local stable manifold of the equilibrium point follows closely the PDLS curve, it is useful to numerically keep track of the PDLS curve to find initial guesses of the parameters to start a shooting search. Numerically, this is done in the following steps.

1. Find the crash-fold on the x-capacity surface by finding the maximal points in variable y for the x-nullcline $f = 0$ which is solved for y as a function of x and z. The projected image on $x = 0$ is used as the initial points for the slow yz-equation of Eq.(6) with $\varepsilon = 0$ and $x = 0$.

2. The yz-slow equation is changed to a first order equation using y as the independent variable and z as the dependent variable: $dz/dy = zh/yg$, starting at point of the projected capacity fold (PCF) to $y = 0$. The 4th order Runge-Kutta method with 150 steps of discretization is used to find the solution $z = z(y)$.

3. The discrete points of the solution above is used to generate the integral of the PDLS equation by the Simpson's rule for integration, and the PDLS point y_{pdls} is solved from the equation.

4. The z-component of the PDLS curve is obtained by finding the corresponding z-value $z = z(y_{pdls})$.

Parameter Regions: Plausible initial guesses for parameter values need to yield the following configuration for the nullcline surfaces of the system. (1) The x-nullcline surface $f = 0$ must fold in y. (2) The nontrivial y-nullcline on the x-capacity surface $f = 0$ must start with a survival threshold branch from its own transcritical point on $y = 0$. (3) The coexisting equilibrium point p_f needs to be on the y-survival threshold branch on the x-capacity surface. (4) The PDLS curve needs to move across the equilibrium point as some parameter value changes. For configuration (1) we try to make the x-transcritical point, $f(0, y, 0) = 0$, lower on the y-axis when $x = z = 0$. Assume y is small enough, then $1 - y \sim 1$ and we can express y from $f(0, y, 0) = 0$ roughly as $y \sim (\frac{m_1}{a_1+1} - 1)\frac{a_2}{m_2}$. Therefore, for large enough m_1, we can guarantee $y_{trn} > 0$ and more importantly we can use a_2 as a changing parameter to lower or to raise the TRN curve which in turn lower or raise the PDLS curve strategically at least at one z-section with $z = 0$. This choice in a_2 (or m_2 similarly) also leads to a realization of (4). Similarly, for configuration (2), the y-transcritial point on $y = 0$ on the x-capacity surface is $g(x, 0, z) = 0, f(x, 0, z) = 0$, which can be solved

in z as $z = (\frac{m_2 x}{a_2+x} - 1)\frac{a_3}{m_3}$ with $x \sim 1$. Thus, making a_3 small (or m_3 large) enough guarantees the transcritial point starts the y-survival threshold branch. As for (3), since the z-nullcline can be solved explicitly as $y = \frac{a_3}{m_3-1}$, similar choices in a_3 (respectively m_3) will force the equilibrium point p_f on the unstable branch of the y-nullcline, which also make it an unstable spiral for the yz-slow dynamics on the x-slow manifold by the slow dynamics analysis above. In conclusion, one should start out by trying some fair values of m_i and small values of a_j for sufficiently small ε. Once a homoclinic orbit is found for small ε we then try to continue it to its native value $\varepsilon = 1$ by varying a_2, which moves the PDLS up and down effectively.

5. Result. Figure 4 shows the result of one search by the search algorithm. Fig.4(a,b) shows the result for a small value of the auxiliary singular parameter $\varepsilon = 0.01$. The corresponding attraction of the coexisting equilibrium point to the x-slow manifold can be gauged from the eigenvalues of the linearization of the vector field at the equilibrium point. They are $\lambda_s = -5589.7974$ and $\lambda_u = 0.2915 \pm 1.5986i$ respectively, a magnitude of 10^5 folds for the attraction relative to the expansion. As a result, we can clearly see the singular perturbation effect of the auxiliary system for which the global unstable manifold of the equilibrium point returns towards the slow manifold along the predicted PDLS curve as the turning points. The homoclinic orbit is found by searching the a_2 parameter interval $[0.7, 2]$ with the following searching parameters: The local stable and unstable manifolds are originated from a $\delta = 5 \times 10^{-4}$ neighborhood of the equilibrium point. The common cross-section where the global stable and unstable manifolds meet is $2x + y + z = 1$. The error in y-direction between the global stable and unstable manifolds W^s, W^u on the cross-section is 6.2755×10^{-4}. The homoclinic orbit's closest return to the equilibrium point is within a distance $E_e = 9.2883 \times 10^{-4}$. Only 4 search iterations were carried out to obtain the above result. The search algorithm stopped by the Matlab `ode15s` solver for stiff systems of ordinary differential equations because it cannot meet the preset double precision (10^{-16}) requirement for both relative and absolute errors because of the extreme stiffness of the auxiliary singularly perturbed model. (The backward and forward integrations to obtain the global stable and unstable manifolds, $W^s,\ W^u$ on the shooting plane Σ with the given precisions for the numerical ODE solvers take no more than $9,000$ steps to complete, resulting a total error for each orbit no more than 10^{-8}.) At a first glance, this failure seems unexpected because the singular parameter value is only $\varepsilon = 0.01$. From the eigenvalues of the equilibrium point above we see that the relative stiffness for the system is in the order of 10^{-5}, a substantial stiffness for most ODE solvers.

The stiffness of the system is abated as the singular parameter ε increases to the native value $\varepsilon = 1$ for the chemostat equations Eq.(5). For the same search parameters, the algorithm stopped at the 17th step because the Euclidean error between the global stable and unstable manifolds is $E_s = 1.7323 \times 10^{-8}$, meeting the algorithm's stoppage search error 10^{-6}. The resulting homoclinic orbit error is $E_e = 5.5479 \times 10^{-6}$. (If we were to print the homoclinic orbit on a ten by ten meter poster to get a sense of the accuracy of the shooting method, the returning homoclinic orbit would miss

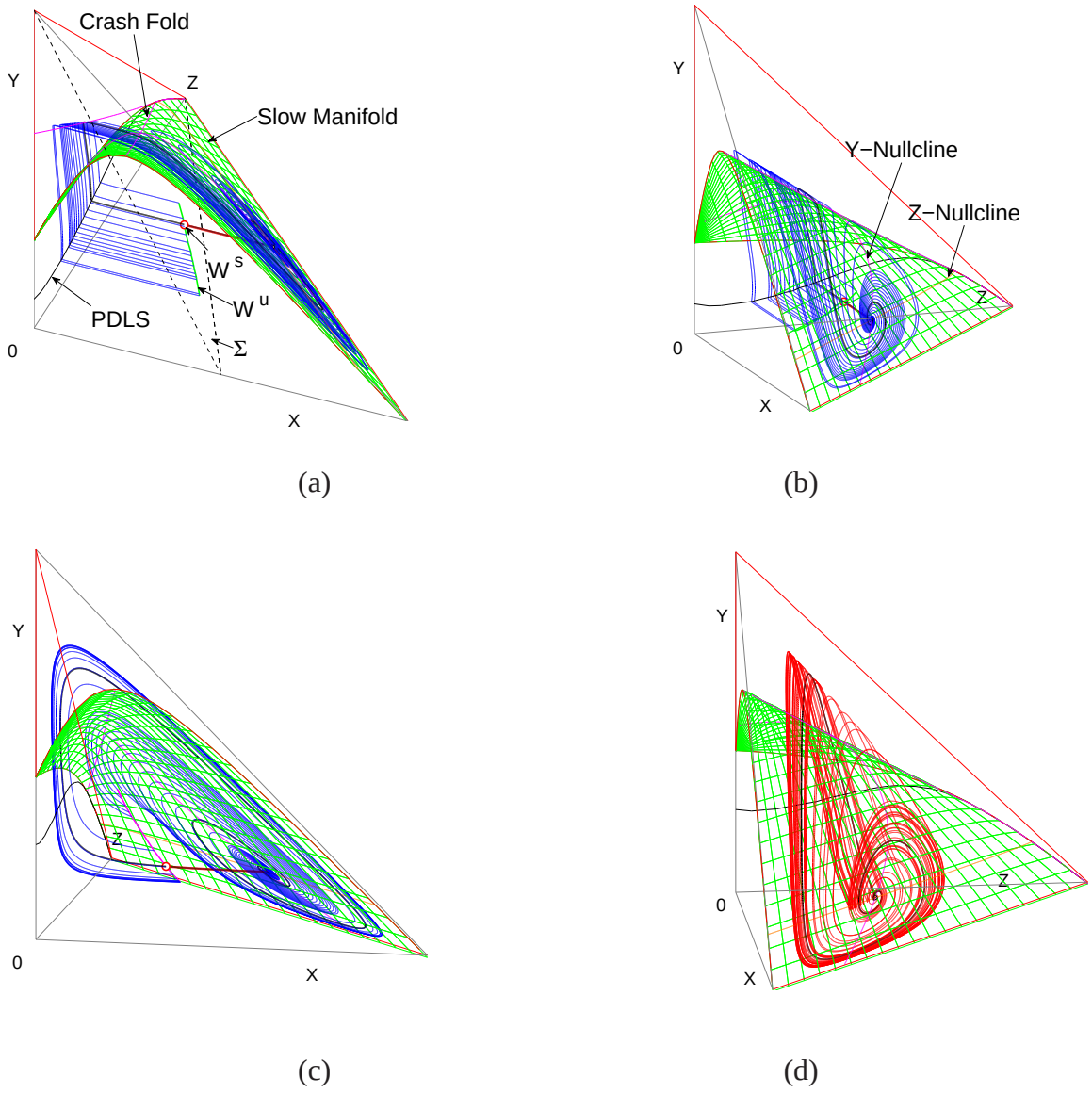

Figure 4: (a) A result of the Shilnikov orbit search algorithm for parameter values of Eq.(5): $\varepsilon = 0.01, a_1 = 0.08, a_2 = 0.110625, a_3 = 0.185, m_1 = 15, m_2 = 5, m_3 = 2.5$. A view showing the returning global unstable manifold connecting the unstable manifold of the equilibrium point. (b) The same phase portrait with a view showing the capacity part of the slow-manifold. (c) With the same parameter values except for the auxiliary singular parameter ε continued to the native value $\varepsilon = 1$ and a new a_2 parameter value 0.170834503173828, a Shilnikov's orbit is found by the search algorithm also. (d) The phase portrait of the attractor by continuing the numerical Shilnikov orbit of (c).

the equilibrium point no more than one centimeter. Also, with the homoclinic starting from a point about one centimeter to the equilibrium point, it should have about 10 full spirals before returning.)

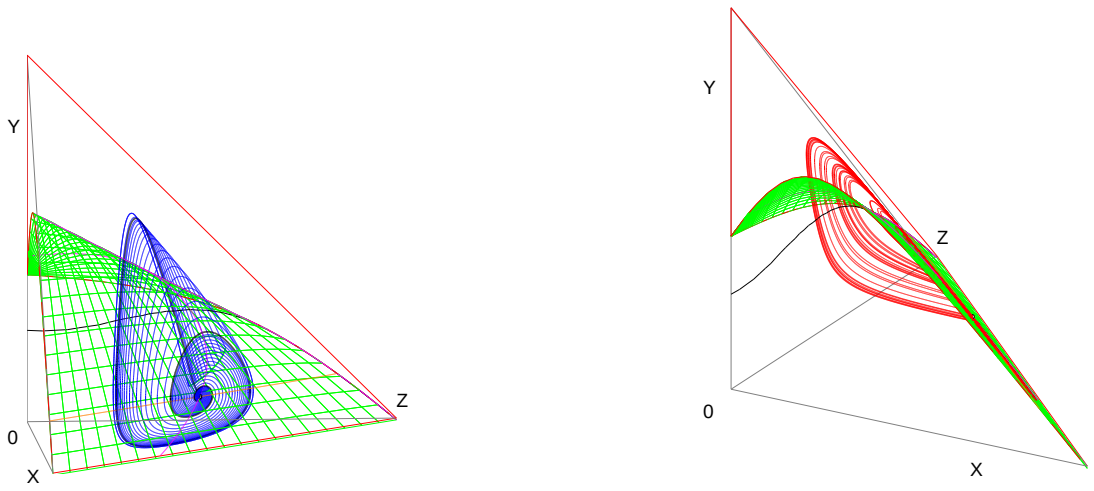

(a) (b)

Figure 5: Parameter values for Eq.(5) are : $\varepsilon = 1, a_1 = 0.08, a_2 = 0.229486083984375, a_3 = 0.185, m_1 = 15, m_2 = 7, m_3 = 2.5$. (a) The unstable manifold and the Shilnikov orbit with $E_e = 4.8 \times 10^{-6}$. (b) The attractor approximated by continuing the numerical Shilnikov orbit.

The stable and unstable eigenvalues of the equilibrium points are $-66.9310, 0.3015 \pm 1.4890i$ respectively, giving a moderate stiffness at the order of 10^{-2}. The homoclinic orbit and the attractor are shown in Fig.4(c,d). It shows clearly that the global unstable manifold returns towards the x-slow manifold at some distance away from the PDLS curve. This suggests that without the auxiliary system's help finding an initial guess of the parameter for a Shilnikov's homoclinic orbit for the original system would be a blind random search.

Using the auxiliary singularly perturbed model is only a sufficient way to locate Shilnikov's orbits. There are such orbits which can be found by the shooting method but is not the result of a continuation of singular Shilnikov orbits as the auxiliary singular parameter ε increases to 1. The orbit found in Fig.5 is such an example. We first located a parameter region where a Shilnikov's orbit might exist for the chemostat model and ran the shooting method to find the a_2 value for such an orbit. But it turns out that this orbit does not persist for the auxiliary singularly perturbed model with small $0 < \varepsilon \ll 1$. Comparing to others this orbit and its corresponding attractor are further away from the coordinate planes. However, even though the full model is far away from the singularly perturbed caricature, the attractor does exhibit a feature characteristic of singularly perturbed equations. Specifically, as shown in Fig.5(b), the attractor still seems to occupy a thing sheet near the capacity branch of the x-nullcline surface that attracts orbits quickly in the x-direction. It is as if the x-variable is a fast variable of the chemostat model. This feature seems not too surprising because the equilibrium point pulls in the stable manifold more strongly

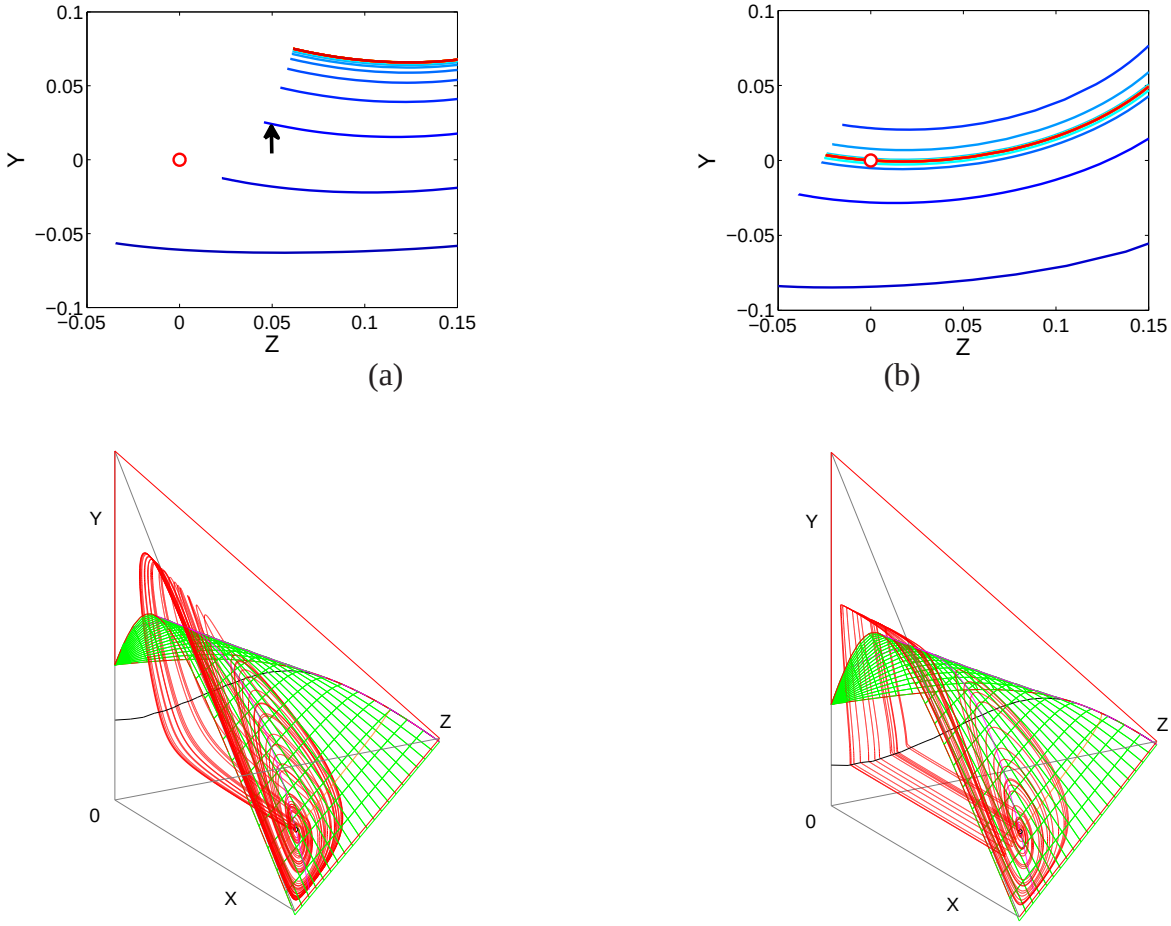

Figure 6: (a) The family of the unstable manifolds W^u and the stable manifold W^s (marker 'o') on the shooting cross-section, with W^s translocated to $(0, 0)$, with a_2 ranging from 0.1 to 0.25. Arrow points at the unstable manifold for the Smith-Waltman parameter values. (b) The same plot for Eq.(6) for parameter values $\varepsilon = 1, a_1 = 0.08, a_3 = 0.20, m_1 = 8, m_2 = 3.2, m_3 = 2.8$ with a_2 ranging from 0.08 to 0.23. A numerical Shilnikov orbit is found for $a_2 = 0.203790740966797$ with the equilibrium point shooting error $E_e = 1.38 \times 10^{-6}$. (c) The attractor approximated by continuing the numerical Shilnikov orbit for $t = 400$. (d) A numerical Shilnikov attractor for the same parameter values except for $\varepsilon = 0.01$ and $a_2 = 0.1481640625$ and $E_e = 3 \times 10^{-4}$.

than pushes out the unstable manifold as the corresponding eigenvalues are $\lambda_s = -55.6448, \lambda_u = 0.4700 \pm 1.7145i$, respectively. The contracting to expanding ratio is of the second order 10^{-2} in magnitude.

Last, let us consider the Smith-Waltman attractor, whose parameter values for Eq.(5) are as in Fig.1(b). We applied our shooting algorithm using a_2 as the searching parameter. The search failed to find a Shilnikov's orbit. Fig.6(a) is the result of the search showing that the search condition

(10) fails to hold: the shooting target W^s is not in the range of the unstable manifold W^u.

This result implies that to find a Shilnikov's orbit near the Smith-Waltman parameter values we need include one more parameter dimension to our search. The rationale for choosing this additional parameter is suggested by the result of Fig.6(a). More specifically, it shows the global unstable manifold swings to the higher end in the z-direction of the stable manifold. Since the returning part of the global unstable manifold orbits increases in the z-direction, it is desirable to compensate this overshot by decreasing the magnitude of the righthand side of the z-equation, i.e., slowing down the z variable. We tried this idea by reducing the m_3 value without success. Instead, we returned to the dimensional model Eq.(3) and considered to change the dimensional parameter w. It can be seen from the change of parameters and variables of Eq.(4) that by increasing the dimensional washout rate w, we can simultaneously decreasing the dimensionless parameters m_1, m_2, m_3. It turned out that this choice of the one dimensional parameter worked. The result is shown in Fig.6(b), for the same Smith-Waltman parameters except that each m_i is scaled by a factor 0.8, corresponding to scaling the washout rate w by a factor of 1.25. Fig.6(c) shows the corresponding chaos attractor. Fig.6(d) shows that the Shilnikov orbit of the neighboring Smith-Waltman parameter can be the continuation of the artificial singularly perturbed model Eq.(6).

6. Conclusion Remark. Biological systems are inherently complex. Simple systems with complex dynamics are attractive for the obvious reasons. Chemostat models are more so because experiments can be readily set up in lab and the mathematics needed for modeling the systems are very simple for both experimentalists and theorists alike. Yet, proving chaos for such seemly simple models is never an easy task. Such problems almost always managed to become a protracted quest for theorists. Proving the existence of a Shilnikov's saddle-focus homoclinic orbit is a good strategy for differential equations. If the systems are singularly perturbed, the problem becomes easier. For the chemostat model considered in this paper we used the geometric method of singular perturbation only as an auxiliary means to locate possible parameter regions and then to find such chaos generating orbits numerically.

In fact, our result, c.f. Fig.6(b) can be considered as a computer-assisted proof. Specifically, the local stable and unstable manifolds are approximated within an error of 10^{-8}. The local manifolds are globally extended in finite times to the shooting plane Σ to be W^s, W^u, respectively. Because the extension times are finite (no more than $9,000$ steps with both relative and absolution precisions set at 10^{-16} for the numerical solver used), the errors are controlled within a margin no more than 10^{-4}. As can be seen from Fig.6(b) that the family of the stable manifolds parameterized by the shooting parameter a_2 is inside a region filled by the family. Actually, the stable manifold family W^s is all translated to one point on the shooting plane, conveniently at the origin $(0, 0)$, which as shown is bounded away from the boundary of the unstable manifold family in distance at least of the order 10^{-2}, a robust zone at least two orders of magnitude greater than the margin of error. Therefore, it must be inside the region filled by the unstable manifold family W^u. As a result,

by an intermediate value theorem argument, the unstable manifold family must sweep the entire region between the top and the bottom boundaries and one member of the family must intersect the stable manifold, i.e. $W^s \in W^u$, proving the existence of a Shilnikov's saddle-focus homoclinic orbit outside the margins of numerical error. As a consequence, the chemostat model is chaotic in the sense of the block shift dynamical systems for the corresponding parameter values. Although this is not an analytical proof, it is a computer-assisted proof nonetheless.

As a last note, this method *in silico* should be easily adapted for other systems, e.g. [26, 27] which are resistive to analytical treatment for chaos generation. Also, it is our hope that the numerical method perhaps some day in the future can be made into an analytical proof. As pointed out early, one theoretical difficulty lies in expressing the Pontryagin's delay of lost stability curve as a function of the parameters in order to show its crossing with the equilibrium point for the singular perturbation case. And the other theoretical difficulty lies in the continuation of a singular homoclinic orbit to the large chemostat value of the singular parameter for the original system.

Acknowledgement: The first author acknowledges the generous visitor fellowships in 2010 from the Department of Mathematics, Tsinghua University, Taiwan, and in 2015 from the Mathematics and Science College, Shanghai Normal University, Shanghai, China. The second author was partially supported by two NNSF grants of China (No.1271261 and No.11431008) for this research.

References

[1] J. Monod, "The growth of bacterial cultures," *Annual Reviews in Microbiology*, vol. 3, no. 1, pp. 371–394, 1949.

[2] A. Novick and L. Szilard, "Experiments with the chemostat on spontaneous mutations of bacteria," *Proceedings of the National Academy of Sciences*, vol. 36, no. 12, pp. 708–719, 1950.

[3] S.-B. Hsu, S. Hubbell, and P. Waltman, "A mathematical theory for single-nutrient competition in continuous cultures of micro-organisms," *SIAM Journal on Applied Mathematics*, vol. 32, no. 2, pp. 366–383, 1977.

[4] H. L. Smith and P. Waltman, *The theory of the chemostat: dynamics of microbial competition*, vol. 13. Cambridge University Press, 1995.

[5] G. Butler, S. Hsu, and P. Waltman, "Coexistence of competing predators in a chemostat," *Journal of Mathematical Biology*, vol. 17, no. 2, pp. 133–151, 1983.

[6] K.-S. Cheng, "Uniqueness of a limit cycle for a predator-prey system," *SIAM Journal on Mathematical Analysis*, vol. 12, no. 4, pp. 541–548, 1981.

[7] Y. Kuang, "Limit cycles in Gause-type predator-prey systems," *University of Alberta*, 1988.

[8] S. Hsu, S. Hubbell, and P. Waltman, "Competing predators," *SIAM Journal on Applied Mathematics*, vol. 35, no. 4, pp. 617–625, 1978.

[9] S. Hsu, S. Hubbell, and P. Waltman, "A contribution to the theory of competing predators," *Ecological Monographs*, vol. 48, no. 3, pp. 337–349, 1978.

[10] W. Liu, D. Xiao, and Y. Yi, "Relaxation oscillations in a class of predator–prey systems," *Journal of Differential Equations*, vol. 188, no. 1, pp. 306–331, 2003.

[11] A. Hastings and T. Powell, "Chaos in a three-species food chain," *Ecology*, vol. 72, no. 3, pp. 896–903, 1991.

[12] P. Hogeweg and B. Hesper, "Interactive instruction on population interactions," *Computers in Biology and Medicine*, vol. 8, no. 4, pp. 319–327, 1978.

[13] B. Deng, "Food chain chaos due to junction-fold point," *Chaos: An Interdisciplinary Journal of Nonlinear Science*, vol. 11, no. 3, pp. 514–525, 2001.

[14] B. Deng and G. Hines, "Food chain chaos due to Shilnikovs orbit," *Chaos: An Interdisciplinary Journal of Nonlinear Science*, vol. 12, no. 3, pp. 533–538, 2002.

[15] B. Deng and G. Hines, "Food chain chaos due to transcritical point," *Chaos: An Interdisciplinary Journal of Nonlinear Science*, vol. 13, no. 2, pp. 578–585, 2003.

[16] S. Smale, "On the differential equations of species in competition," *Journal of Mathematical Biology*, vol. 3, no. 1, pp. 5–7, 1976.

[17] A. J. Lotka, "Elements of physical biology," *Science Progress in the Twentieth Century (1919-1933)*, vol. 21, no. 82, pp. 341–343, 1926.

[18] A. Lotka, "Fluctuations in the abundance of species considered mathematically (with comment by V. Volterra)," *Nature*, vol. 119, pp. 12–13, 1927.

[19] V. Volterra, "Fluctuations in the abundance of a species considered mathematically," *Nature*, vol. 118, pp. 558–560, 1926.

[20] S. Smale, "Diffeomorphisms with many periodic," in *Differential and combinatorial topology: A symposium in honor of Marston Morse*, vol. 27, p. 63, Princeton University Press, 1965.

[21] M. L. Cartwright and J. E. Littlewood, "On non-linear differential equations of the second order: I. the equation ÿ - k(1 - y^2) ẏ + y = bλk cos(λl+α), k large," *Journal of the London Mathematical Society*, vol. 1, no. 3, pp. 180–189, 1945.

[22] N. Levinson, "A second order differential equation with singular solutions," *Annals of Mathematics*, pp. 127–153, 1949.

[23] P. Yu, M. Han, and D. Xiao, "Four small limit cycles around a Hopf singular point in 3-dimensional competitive Lotka–Volterra systems," *Journal of Mathematical Analysis and Applications*, vol. 436, no. 1, pp. 521–555, 2016.

[24] B. Deng, "Food chain chaos with canard explosion," *Chaos: An Interdisciplinary Journal of Nonlinear Science*, vol. 14, no. 4, pp. 1083–1092, 2004.

[25] B. Deng and I. Loladze, "Competitive coexistence in stoichiometric chaos," *Chaos: An Interdisciplinary Journal of Nonlinear Science*, vol. 17, no. 3, p. 033108, 2007.

[26] M. E. Gilpin, "Spiral chaos in a predator-prey model," *The American Naturalist*, vol. 113, no. 2, pp. 306–308, 1979.

[27] K. Mccann and P. Yodzis, "Bifurcation structure of a three-species food-chain model," *Theoretical Population Biology*, vol. 48, no. 2, pp. 93–125, 1995.

[28] B. Bockelman and B. Deng, "Food web chaos without subchain oscillators," *International Journal of Bifurcation and Chaos*, vol. 15, no. 11, pp. 3481–3492, 2005.

[29] S. Muratori and S. Rinaldi, "Low-and high-frequency oscillations in three-dimensional food chain systems," *SIAM Journal on Applied Mathematics*, vol. 52, no. 6, pp. 1688–1706, 1992.

[30] L. Shilnikov, "The existence of a denumerable set of periodic motions in four-dimensional space in an extended neighborhood of a saddle-focus," in *Soviet Math. Dokl*, vol. 8, pp. 54–58, 1967.

[31] L. Šil'nikov, "A contribution to the problem of the structure of an extended neighborhood of a rough equilibrium state of saddle-focus type," *Mathematics of the USSR-Sbornik*, vol. 10, no. 1, p. 91, 1970.

[32] C. Tresser, "About some theorems by LP Šil'nikov," in *Annales de l'IHP Physique théorique*, vol. 40, pp. 441–461, 1984.

[33] B. Deng, "On Šil'nikov's homoclinic-saddle-focus theorem," *Journal of Differential Equations*, vol. 102, no. 2, pp. 305–329, 1993.

[34] B. Deng, "Exponential expansion with principal eigenvalues," *International Journal of Bifurcation and Chaos*, vol. 6, no. 06, pp. 1161–1167, 1996.

[35] B. Deng, "Constructing homoclinic orbits and chaotic attractors," *International Journal of Bifurcation and Chaos*, vol. 4, no. 04, pp. 823–841, 1994.

[36] B. Deng, "Constructing lorenz type attractors through singular perturbations," *International Journal of Bifurcation and Chaos*, vol. 5, no. 06, pp. 1633–1642, 1995.

[37] C. S. Holling, "Some characteristics of simple types of predation and parasitism," *The Canadian Entomologist*, vol. 91, no. 07, pp. 385–398, 1959.